Cerebral Cortex December 2009;19:2902–2915
doi:10.1093/cercor/bhp060
Advance Access publication April 9, 2009

Axon Morphologies and Convergence Patterns of Projections from Different Sensory-Specific Cortices of the Anterior Ectosylvian Sulcus onto Multisensory Neurons in the Cat Superior Colliculus

Veronica Fuentes-Santamaria, Juan C. Alvarado, John G. McHaffie and Barry E. Stein

Department of Neurobiology and Anatomy, Wake Forest University School of Medicine, Winston-Salem, NC 27157, USA

Corticofugal projections to the thalamus reveal 2 axonal morphologies, each associated with specific physiological attributes. These determine the functional characteristics of thalamic neurons. It is not clear, however, whether such features characterize the corticofugal projections that mediate multisensory integration in superior colliculus (SC) neurons. The cortico-collicular projections from cat anterior ectosylvian sulcus (AES) are derived from its visual, auditory, and somatosensory representations and are critical for multisensory integration. Following tracer injections into each subdivision, 2 types of cortico-collicular axons were observed. Most were categorized as type I and consisted of small-caliber axons traversing long distances without branching, bearing mainly small boutons. The less frequent type II had thicker axons, more complex branching patterns, larger boutons, and more complex terminal boutons. Following combinatorial injections of 2 different fluorescent tracers into defined AES subdivisions, fibers from each were seen converging onto individual SC neurons and indicate that such convergence, like that in the corticothalamic system, is mediated by 2 distinct morphological types of axon terminals. Nevertheless, and despite the conservation of axonal morphologies across different subcortical systems, it is not yet clear if the concomitant physiological attributes described in the thalamus are directly applicable to multisensory integration.

Keywords: auditory, cross-modal, drivers, modulators, multimodal, somatosensory, visual

Introduction

Multisensory neurons in the cat superior colliculus (SC) play a significant role in mediating orientation to cues from different senses (Stein and Meredith 1993). These neurons are rendered multisensory via converging afferents from morphologically and functionally diverse unisensory structures (Edwards et al. 1979; Huerta and Harting 1984; Stein and Meredith 1991; Wallace et al. 1993). They also are able to engage in multisensory integration and thereby synthesize these different sensory inputs. This process allows SC neurons to markedly enhance or degrade their responses (see Stein and Stanford 2008 for a review) and to influence orientation behaviors via their descending projections to premotor and motor nuclei in the brainstem and spinal cord (Grantyn and Grantyn 1982; Huerta and Harting 1982; Guitton and Munoz 1991; Munoz and Guitton 1991; Meredith et al. 1992). Consequently, the stimulus conditions that enhance or degrade the activity of SC multisensory output neurons also enhance or degrade the likelihood of orientation to events generating cross-modal cues (Stein et al. 1988, 1989; Wilkinson et al. 1996; Jiang et al. 2002; Burnett et al. 2004).

However, SC neurons do not have an intrinsic capability to engage in multisensory integration but rather depend on influences from the anterior ectosylvian sulcus (AES), a region of association cortex which projects heavily to the multisensory (deep) layers of the SC (Stein et al. 1982; McHaffie et al. 1988; Meredith and Clemo 1989; Harting et al. 1997). This cortical area is divided into 3 largely unisensory regions; the anterior ectosylvian visual region (AEV, see Mucke et al. 1982; Olson and Graybiel 1987); the auditory field of AES (FAES, see Clarey and Irvine 1986; Meredith and Clemo 1989); and the fourth somatosensory area (SIV, see Clemo and Stein 1982, 1983). Each subdivision sends unisensory projections to converge on their target SC neurons in patterns that match their modality-convergence profiles from other sources (e.g., AEV and FAES converge on visual-auditory SC neurons; see Wallace et al. 1993). Temporarily removing AES influences via reversible cortical deactivation precludes multisensory integration in SC neurons. Thus, they no longer exhibit responses to the cross-modal stimuli that exceed those to the most effective of its individual component stimuli (Wallace and Stein 1994; Jiang et al. 2001; Alvarado et al. 2007) and SC-mediated multisensory behaviors also are disrupted (Wilkinson et al. 1996; Jiang et al. 2002). These effects are induced without abolishing SC responses to the individual component stimuli of a cross-modal stimulus combination (Wallace and Stein 1994; Jiang et al. 2001; Alvarado et al. 2007). In short, SC neurons remain multisensory but cannot integrate their different sensory inputs to enhance overt behavior without inputs from the AES.

Anatomical studies of corticofugal fibers terminating in both sensory (Sherman and Guillery 1998; Guillery et al. 2001; Huppé-Gourgues et al. 2006) and motor (Kultas-Ilinsky et al. 2003) regions of the thalamus indicate that 2 types of axonal and terminal morphologies characterize corticothalamic projections. In visual thalamic areas, these 2 fiber types have been associated with different physiological attributes (Guillery and Sherman 2002; Sherman and Guillery 2002; Sherman 2007) that differentially shape the response characteristics of corticothalamic neurons. Whether similar corticofugal axonal morphologies are involved in providing the AES influences critical for multisensory integration in the SC is not yet known, but the functional properties associated with these specific morphological projections might be directly applicable to the AES–SC projection. Unfortunately, little is known about the morphology of these projections and/or whether such specialized projections are adapted to a variety of cortical-subcortical systems or are unique to the corticothalamic system. Thus, we sought to test the possibility that these axonal morphologies also characterize the cortico-collicular system. Cortico-collicular terminals from AES

were labeled using biotinylated dextran amine (BDA) injections into physiologically defined subdivision of AES. To evaluate the manner in which the fibers from different AES subdivisions converge onto individual SC output neurons, paired injections of different fluorescent tracers were made in different AES subdivisions, and SC output neurons were identified by immunostaining with an antibody directed against the non-phosphorylated form of neurofilament H protein SMI-32 (Fuentes-Santamaria et al. 2006). The data reveal a heretofore unappreciated complexity in the axonal morphology of cortico-collicular fibers and provide the first anatomical demonstration of multisensory convergence on SC neurons.

Material and Methods

Experimental Subjects

Twenty-nine cats were used in the present study. All the experimental procedures were conducted following the National Institutes of Health "Guide for the Care and Use of Laboratory Animals" (NIH Publications No. 80-23, revised 1996) and were approved by the Institutional Animal Care and Use Committee at Wake Forest University School of Medicine. Efforts were made to minimize the number of animals used. All animals received appropriate anesthetics and analgesics to mitigate pain and suffering (see below).

Surgery and Tracer Injections

Animals were sedated with ketamine hydrochloride (30 mg/kg, im) and acepromazine maleate (0.3–0.5 mg/kg, im), intubated through the mouth, and then anesthetized for surgery with isoflurane (0.5–3%). During surgery, body temperature was maintained with a heating pad. Animals were positioned in a stereotaxic head-holder, and a craniotomy was performed to expose the AES. The antero-posterior and medio-lateral boundaries of AEV, FAES, and SIV were mapped physiologically using a tungsten microelectrode (1–3 MΩ) moved across the cortex in a grid-like pattern. At each sampled locus, the electrode was lowered through cortex (1–2.5 mm), and the properties of single neurons and multineuron clusters were examined in response to visual, auditory and somatosensory search stimuli. Visual search stimuli consisted of a moving or flashed light; auditory search stimuli included broadband (20–20,000 Hz) noise bursts, clicks, claps, and whistles; and somatosensory search stimuli consisted of mechanical taps, manual compression of the skin and rotation of joints. Each site was characterized as visual, auditory, somatosensory or multisensory. Multisensory zones were generally transitional between 2 primarily modality-specific zones as previously described (Wallace et al. 1993). Transitions from one zone to another were noted and marked stereotaxically. Once the AES subdivisions were delineated, the needle tip of a 10-μL Hamilton syringe was placed in the middle of a subdivision and lowered to a depth of 1–1.5 mm. All the tracers used in the present study, including dextran amine (Molecular Probes, Eugene, OR) conjugated to biotin (BDA), Alexa-594 (Molecular Probes), or Alexa-488 (Molecular Probes), were dissolved in phosphate buffer (PB) to yield a concentration of 10% and pressure injected to yield a deposit of approximately 2 μL. Following the injection, the syringe was left in place for 15 min to minimize the migration of the tracer along the needle tract during its removal. After needle removal, the incision was sutured. Postsurgical analgesic (butorphanol tartrate, 0.1–0.4 mg/kg/6 h) was administered as needed, and an antibiotic (ceftriaxone, 20 mg/kg/bid) was given for 7–10 days.

BDA Tracer Injection and SMI-32 Immunostaining: Double-Labeling Studies

In order to examine the morphology of AES terminals as well as their distribution onto output neurons, the SC of animals receiving BDA cortical injections also was processed for SMI-32 immunohistochemistry that previously has been shown to preferentially label SC output neurons in the cat (Fuentes-Santamaria et al. 2006). After a 10-day survival period, animals (n = 9) were sedated with ketamine hydrochloride (30 mg/kg, im) and acepromazine maleate (0.3–0.5 mg/kg, im). Thirty min later, they were anesthetized with sodium pentobarbital (100 mg/kg ip) and, following the loss of pinnae reflexes, were perfused transcardially with 0.9% saline wash followed by a fixative solution of 4% paraformaldehyde in 0.1 M PB, pH 7.3. Brains were blocked stereotaxically in situ, removed, stored overnight at 4 °C in the same fixative solution, and then sectioned coronally at 50 μm on a vibratome. To identify BDA-stained fibers, sections were rinsed 4 times for 15 min in phosphate-buffered saline (PBS) and then incubated in the biotin–avidin peroxidase complex (ABC) for 2 h at room temperature (RT). The peroxidase was visualized with a nickel-intensified diaminobenzidine (DAB) reaction to produce a black reaction product. For SMI-32 immunocytochemistry, sections were preincubated for 1 h in 10% normal goat serum (NGS) and then incubated in SMI-32 monoclonal antibody (1:2500; Sternberger Monoclonals, Inc., Jarrettsville, MD) diluted in PBS containing 0.2% Triton X-100 (Tx) overnight at 4 °C. The following day, after several rinses in PBS-Tx (0.2%), sections were incubated in a dilution of biotinylated anti-mouse secondary antibody (1:200; Vector Laboratories, Burlingame, CA) for 2 h at RT. After washing in PBS-Tx (0.2%), sections were incubated in ABC for 1 h and then reacted with DAB and hydrogen peroxide to produce a brown reaction product.

Dual BDA Tracer Injections and SMI-32 Immunostaining: Triple-Labeling Studies

To determine the convergence patterns between pairs of AES subdivisions onto SC output neurons, 3 sets of experiments were carried out: 1) injections of BDA-594 into the FAES and injections of BDA-488 into the AEV; 2) injections of BDA-488 into the AEV and injections of BDA-594 into the SIV; and 3) injections of BDA-488 into the FAES and injections of BDA-594 into SIV. Sections from dual-injected animals subsequently were processed for SMI-32 immunocytochemistry. Animals (n = 11) were anesthetized as described above. After fixation the brains were blocked stereotaxically, removed, and sectioned at 50 μm on a vibratome in the coronal plane. BDA-fluorescent sections were rinsed several times in PBS-Tx (0.2%) and, in order to reduce nonspecific binding, were blocked for 1 h in the same buffer containing 10% NGS. Sections then were incubated overnight at 4 °C with SMI-32 monoclonal antibody in a solution containing PBS-Tx (0.2%), pH 7.6. After four 15-min rinses in PBS-Tx (0.2%), sections were incubated for 1 h in biotinylated anti-mouse secondary antibody (Vector Laboratories, Burlingame, CA); the staining was visualized by incubation in a solution of PBS-Tx (0.2%) and streptavidin (Molecular Probes, Eugene, OR). Finally, sections were mounted onto gelatin-coated slides, coverslipped using Gel Mount mounting medium (Biomeda, Foster City, CA), and dried overnight at 4 °C.

Electron Microscopy: Double-Labeling Studies

To investigate the ultrastructure of cortico-collicular terminals, pre-embedding techniques were used in AES-injected animals. Animals (n = 9) were anesthetized as described above, perfused transcardially with 0.9% saline wash followed by a fixative perfusion of 4% paraformadehyde and 1% glutaraldehyde in 0.1 M PB, pH 7.3. After fixation, the brains were blocked stereotaxically, removed, and sectioned at 50 μm on a vibratome in the coronal plane. To identify BDA-stained fibers, sections were rinsed 4 times for 15 min in PBS and then incubated in ABC for 3 h at RT. The peroxidase was visualized with a nickel-intensified DAB reaction to produce a black reaction product. After several washes in PBS, sections were preincubated for 1 h in 10% NGS and then incubated overnight at 4 °C with SMI-32 monoclonal antibody diluted in PBS. The following day, after several rinses in PBS, sections were incubated in a dilution of anti-mouse secondary antibody conjugated to 1.4-nm immunogold particles (1:100; NanoProbes, Inc., Stony Brook, NY) for 2 h at RT. After several rinses in distilled water, gold particles were revealed with silver intensification (HQ silver, Nanoprobes, Inc.). Regions containing stained fibers were dissected out, osmicated in 1% osmium tetroxide in 0.1 M PB, rinsed several times in 0.1 M PB, dehydrated in a graded ethyl alcohol series, rinsed in 100% propylene oxide 2 times for 20 min, and placed in 1:1 mixture of Spurr

Resin (Polysciences, Warrington, PA) and propylene oxide overnight. Sections then were transferred to a 1:2 mixture of resin and propylene oxide and finally to a pure mixture of Spurr Resin (3 h) and cured overnight at 70 °C. Thin sections (75 nm) were cut on an ultramicrotome (Reichert-Jung Ultracut E, Leica, Wetzlar, Germany) and mounted on copper grids. Sections were stained with uranyl acetate and lead citrate for 10 min each. Tissue was observed using a Philips 400 TEM (Philips, Eindhoven, the Netherlands).

Immunohistochemical Controls

SC sections were incubated in the absence of SMI-32 primary antibody, which was replaced by either buffer or nonimmune serum from the same species, in order to test the antibody specificity (Burry 2000). No immunostaining was detected under these conditions. The specificity of this antibody has been extensively tested in cat tissue by Western blot (Sternberger and Sternberger 1983; Lee et al. 1988; Van der Gucht et al. 2001).

Nomenclature

The nomenclature used to define AES subdivisions and SC lamination was in accordance with previous studies. Briefly, AES is located at the juncture of the frontal, parietal and temporal regions of the cortex. The somatosensory subdivision, SIV, is located in the anterior dorsal bank (Clemo and Stein 1983), whereas the anterior ectosylvian auditory field (FAES) (Clarey and Irvine 1986; Meredith and Clemo 1989) and the anterior ectosylvian area (AEV) (Mucke et al. 1982; Olson and Graybiel 1987) are located in the anterior dorsal and posterior ventral banks. The SC is a laminated structure usually divided into superficial (visual) and deeper (multisensory) laminae (see Stein and Meredith 1993). The superficial laminae consist of the *stratum zonale*, *stratum griseum superficiale*, and *stratum opticum*, whereas the deeper layers (an amalgam of the intermediate and deep layers) include the *stratum griseum intermediale*, the *stratum album intermedium*, the *stratum griseum profundum*, and the *stratum album profundum* (see Kanaseki and Sprague 1974 for further details).

In the present study, the term *''compartment''* was used when referring to the specific neuron's components; these include the soma, dendrites (primary, secondary or tertiary) and axon. In addition, although an "*apposition''* does not unequivocally denote synaptic contact or synapse (Pilowsky et al. 1992), this term has been used to indicate that a stained terminal and the labeled neuron are in focus in the same focal plane with no detectable gap between them (Pilowsky et al. 1992; El Manira et al. 1997; Makeham et al. 2001). Additionally, *''multisensory integration''* will be defined as the neural processes that are involved in synthesizing information from cross-modal stimuli (Stein and Stanford, 2008).

Data Analysis

Light Microscopy

Images were captured using a Spot RT Slider digital camera (Diagnostic Instruments, Sterling Heights, MI) attached to an Olympus BX50 microscope. Analyses were performed on every fourth labeled section (200 μm), extending through the rostro-caudal extent of the SC. Using a 100× objective, 3 sampling fields (dorsal, middle and ventral; 1 x 10^4 μm^2 each) were defined in the deep layers of each section, and the axon thickness and area of boutons were measured using the public domain image analysis software Scion image for Windows (Scion, Frederick, MD; v beta 4.0.2). Data from all fields in each animal were pooled.

Labeled axons in the deep SC were characterized based on axon thickness, branching patterns, morphology and complexity of bouton arrangements. Labeled boutons were classified into 4 categories based upon size, terminal morphology, and complexity of bouton configuration: 1) boutons on short stalks; 2) *en passant* boutons; 3) boutons *terminaux*; and 4) clustered boutons forming complex configurations. Similar classifications have been used to characterize corticothalamic axons (Rockland 1996; Kultas-Ilinsky et al. 2003) and boutons (Guillery 1966; Guillery et al. 2001; Huppé-Gourgues et al. 2006). Where necessary to reconstruct cortical axons, photomontages were made using multiple focal planes from consecutive sections.

Fluorescence Microscopy

SC fluorescent sections were examined with a BX50 microscope equipped with the fluorescent filters (594-red fluorescence), (350-blue fluorescence), and (488-green fluorescence). Images were captured as indicated above. Analyses of the labeled sections were performed on every fourth section, 200 μm apart. In each section, 3 fields (dorsal, middle and ventral; 25.57 x 10^4 μm^2 each) were sampled using a 20× objective.

Single color images were obtained with each filter, and the 3 images were compiled into a composite image. In order to compare the distribution patterns among neurons receiving converging inputs from FAES-AEV, AEV-SIV, or FAES-SIV, the neuron's center was determined and the distance to each apposition was measured using Scion Image (Scion Corp, Frederick, MD, V. beta 4.0.2). In addition, the percentage of appositions on each cellular compartment (e.g., soma, primary, secondary, and tertiary dendrites) also was calculated.

The soma diameters of SMI-32 immunostained neurons receiving converging cortical inputs were measured using Scion Image for Windows. Three fields (2.97 x 10^4 μm^2; dorsal, middle and ventral) were sampled using a 60× objective in every fourth section of the ipsilateral deep SC throughout the rostro-caudal extent of the nucleus. Only neurons with a well-defined soma, nucleus and nucleolus were measured.

Preparation of Figures and Statistical Analysis

Following the analysis of the data, Photoshop (Adobe Systems, San Jose, CA) and Canvas (ACD Systems, Victoria, British Columbia, Canada) software applications were used to adjust size, brightness and contrast in the preparation of the figures. Image adjustments did not have any effect upon the measurements reported. All data were expressed as mean ± standard deviation and analyzed statistically using ANOVA. Statistical significance was set at $P < 0.05$.

Results

In order to map and delineate AES subdivisions, recording of sensory-evoked responses along the AES were performed and focal deposits of BDA then were made into the central aspects of electrophysiologically delineated sensory-specific subdivisions (Fig. 1). Inspection of injection sites suggests that each was restricted to a single AES subdivision (inserts in Fig. 1*F–H*). Consistent with previous observations (Stein et al. 1983; Norita et al. 1986; McHaffie et al. 1988; Meredith and Clemo 1989; Harting et al. 1997), anterogradely labeled AES fibers were observed predominately in the multisensory layers of the ipsilateral SC. No labeling was present in overlying superficial layers, and only a weak projection to the contralateral SC was apparent.

Classification of Anterogradely Labeled Axons from AES

Following injections of BDA into AES subdivisions, the morphology and synaptic targets of cortico-collicular axons were detailed in the multisensory layers of the SC. Adopting the criteria and nomenclature of Rockland (1996) and Kultas-Ilinsky et al. (2003) for corticothalamic fiber morphology, 2 groups of labeled axons were identified based on axon thickness, branching patterns, morphology and complexity of bouton arrangement. Additionally, in agreement with previous studies characterizing the morphology of corticothalamic boutons (Guillery 1966; Guillery et al. 2001; Huppé-Gourgues et al. 2006), cortical endings were classified into 4 categories according to size, terminal morphology, and complexity of bouton grouping: 1) boutons on short stalks; 2) *en passant* boutons; 3) boutons *terminaux*; and 4) clustered boutons forming complex configurations.

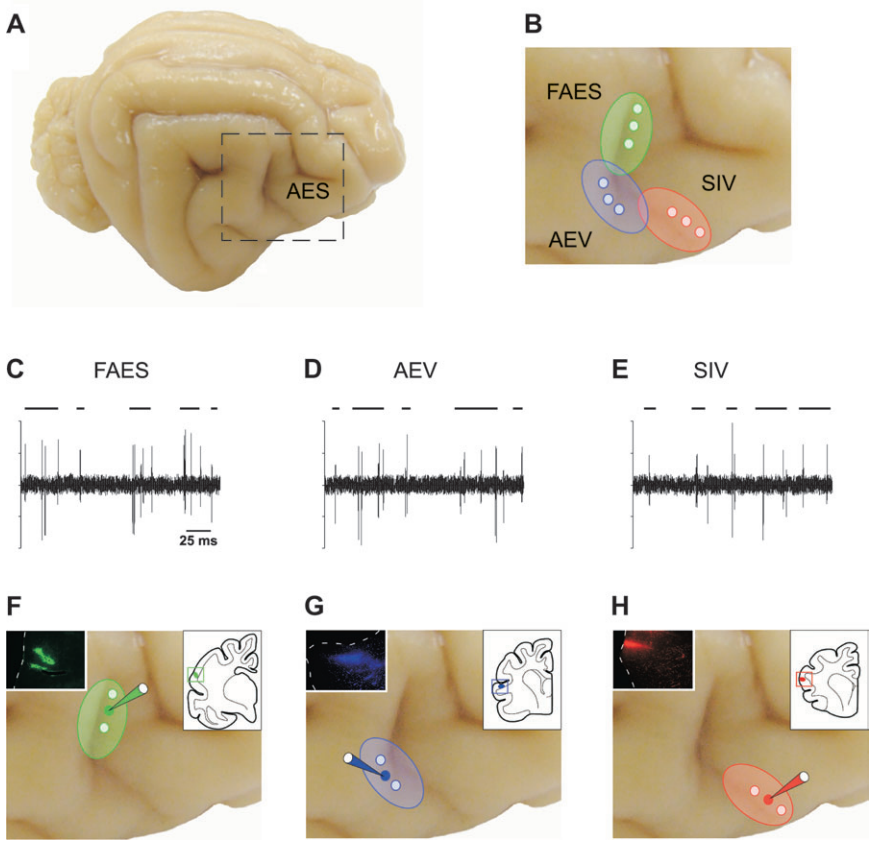

Figure 1. Identification of AES subdivisions and tracer injections of BDA into these cortical subdivisions. The extent and boundaries of FAES, AEV and SIV subdivisions (*A*, *B*) were electrophysiologically identified (*C*–*E*). Auditory search stimuli included broadband (20–20,000 Hz) noise bursts, clicks, claps and whistles (*C*), visual search stimuli consisted of a moving or flashed light (*D*) and somatosensory search stimuli consisted of mechanical taps, manual compression of the skin and rotation of joints (*E*). Once the AES subdivisions were delineated, a small injection of BDA was made in the middle area of the corresponding mapped cortical subdivision (solid circles in *F*–*H*). Drawings at the top right corner in (*F*–*H*) indicate the location of the injection sites into FAES (*F*), AEV (*G*), and SIV (*H*) shown in the same images at the top left corner. Circles in B indicate the electrophysiologically mapped areas in each cortical subdivision.

The first group (type I) was comprised of small-caliber (1.04 ± 0.23 μm diameter) axons that traveled long distances without branching (Fig. 2*A*). These axons bore mainly small boutons on thin short side stalks (white arrowheads in Fig. 2*D*), *en passant* boutons (white arrowheads in Fig. 2*E*,*F*), or single boutons on the terminus of these branches (white arrowheads in Fig. 2*G*,*H*). Other type I axons presented boutons that were distributed sparsely along their course before ramifying into short secondary branches that bore small-sized boutons with morphologic features similar to those described above (Fig. 2*B*,*C*; also see Fig. 2*D*–*H*).

By contrast, a second group (type II) was characterized by large-caliber (2.49 ± 0.63 μm diameter) axons that displayed more complex branching patterns and bouton groupings (Fig. 3). Some of these thick axons ramified into thinner branches before forming terminal arbors of varied complexity with numerous clustered boutons (Fig. 3*A*–*D*). Commonly, these medium to large sized swellings were *en passant* boutons (white arrowheads in Fig. 3*E*), boutons *terminaux* (white arrowheads in Fig. 3*F*,*G*) or medium to large clustered boutons (white arrowheads in Fig. 3*H*,*I*) that could form rosette-like configurations (white arrowheads in Fig. 3*J*,*K*) or more complex structures (white arrowheads in Fig. 3*L*,*M*). Close inspection of these axons revealed no discernable differences in their morphology among AES modality-specific subdivisions. It is important to note however, that although the proportions of these 2 types of cortico-collicular axons were not quantified in the present study, qualitative observations indicate that the majority of AES afferents to the multisensory layers of the SC were type I axons.

In order to evaluate whether there were differences in the morphologic characteristic of boutons among AES modality-specific subdivisions, the size of the boutons on projections from AEV, FAES, and SIV was calculated for each bouton category. As shown in Figure 4, no significant differences in the size of boutons on short stalks (AEV = 2.248 ± 0.822, n = 75; FAES = 2.300 ± 0.882, n = 96; SIV = 2.444 ± 0.714, n = 95; ANOVA, $F_{2,263}$ = 1.39, P > 0.05; Fig. 4*A*), *en passant* boutons (AEV = 2.627 ± 1.593, n = 202; FAES = 2.924 ± 2.295, n = 192; SIV = 2.890 ± 1.595, n = 160; ANOVA, $F_{(2,551)}$ = 1.48, P > 0.05; Fig. 4*B*), boutons *terminaux* (AEV = 3.626 ± 1.654, n = 129; FAES = 3.685 ± 1.821, n = 109; SIV = 4.035 ± 1.683, n = 117; ANOVA, $F_{2,352}$ = 1.98, P > 0.05; Fig. 4*C*), or boutons forming complex configurations (AEV = 6.941 ± 2.688, n = 60; FAES = 7.352 ± 2.524, n = 60; SIV = 6.859 ± 2.473, n = 57; ANOVA, $F_{2,174}$ = 0.63, P > 0.05; Fig. 4*D*) were found among AES subdivisions. The mean area for each bouton category of each AES modality-specific subdivision is shown in Figure 4*E*. Note that, regardless of the AES subdivision of origin, clustered boutons had the largest areas whereas boutons on short stalks had the smallest. Also note the similarity in the mean values for

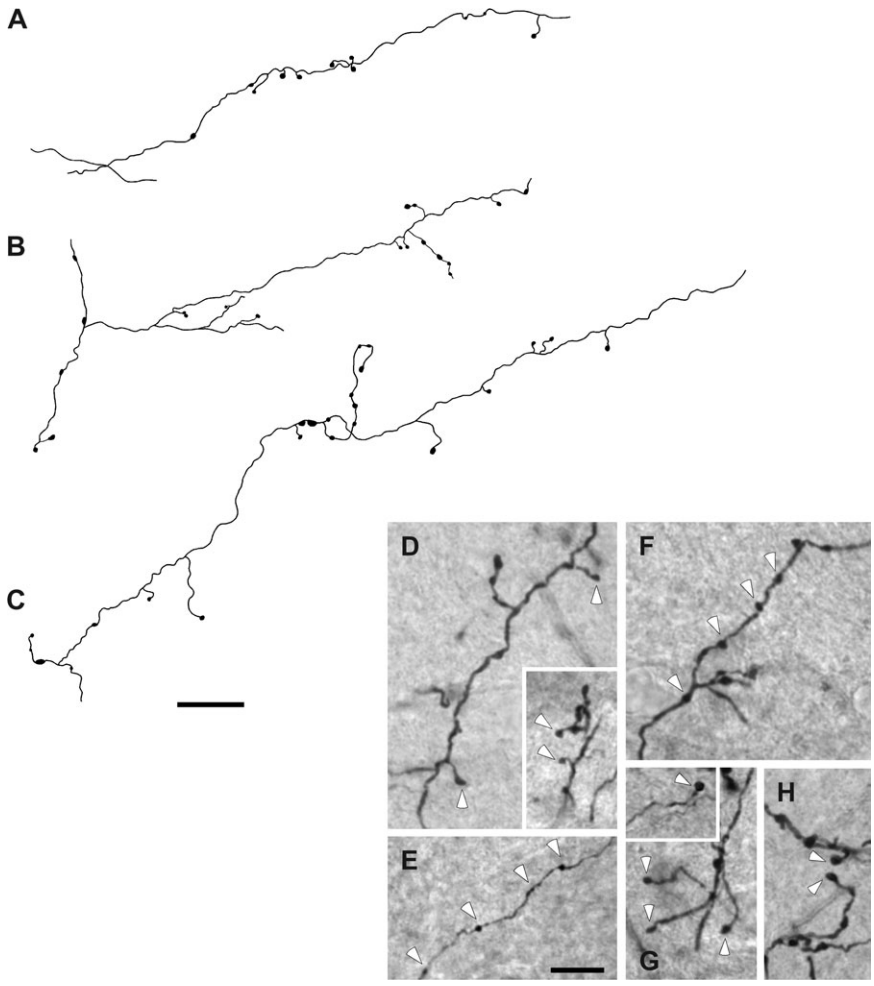

Figure 2. Examples of type 1 axon terminal fields in the deep layers of the SC. These axons were very thin in diameter and gave off few axonal branches along their courses. These branches had sparse swellings (*A–C*) that were mainly small to medium sized boutons on thin short stalks (arrowheads in *D*), *en passant* boutons (arrowheads in *E*, *F*), and also single boutons on the terminus of these branches (arrowheads in *G*, *H*). Scale bar = 25 μm in (*C*); 10 μm in (*E*).

the different boutons categories among AES modality-specific subdivisions (Fig. 4*E*).

Cortical Boutons with Different Morphology and Complexity Appose SMI-32 Immunostained Output Neurons in the Deep SC

To evaluate the relationship between the synaptic morphology of AES cortico-collicular axons and their target multisensory SC neurons, tissue containing BDA-labeled fibers was double-labeled with the SMI-32 antibody. We have shown previously that this antibody, labels the dendritic arbors of SC output neurons far more extensively than other immunohistochemical markers and is preferentially expressed by SC output neurons that project to regions of the brainstem (Fuentes-Santamaria et al. 2006). Additionally, to further characterize the nature of this projection, and to establish whether the appositions seen at the light level were indicative of synaptic contacts with SC output neurons, BDA-labeled AES terminals were examined with electron microscopy (see Methods for a detailed description of double-labeling studies for light and electron microscopy).

Light Microscopy

Terminals from the different AES modality-specific subdivisions were observed apposing SMI-32 immunostained neurons, and a representative example following a BDA injection into AEV is shown in Figure 5. Small boutons linked to thin axons by short stalks, *en passant* boutons, boutons *terminaux* as well as complex bouton configurations were observed apposing various parts of the neuronal architecture. These include the soma (yellow arrows in Fig. 5*A–D*) as well as the primary (blue arrows in Fig. 5*E–H*), secondary (orange arrows in Fig. 5*I–L*), and tertiary dendrites (green arrows in Fig. 5*M–P*). No noticeable differences in the distribution of boutons on SMI-32 immunostained neurons were observed among AES subdivisions.

Electron Microscopy

Cortico-collicular terminals contained several mitochondria and a moderate number of round vesicles (Norita et al. 1986; Harting et al. 1997). They made asymmetrical synaptic contacts with modest postsynaptic densities (black arrowheads in Fig. 6). Generally, terminals from FAES (CT in Fig. 6*A*,*B*), AEV (CT in Fig. 6*C*,*D*), and SIV (CT in Fig. 6*E*), were presynaptic to the dendrites and spines of SMI-32 immunostained output neurons (white arrowheads in Fig. 6 are pointing to silver-intensified immunogold labeled particles).

As previously shown for the SIV (Harting et al. 1997), the synaptic arrangements of AES cortico-collicular axons varied in their complexity. In some instances, cortical terminals made

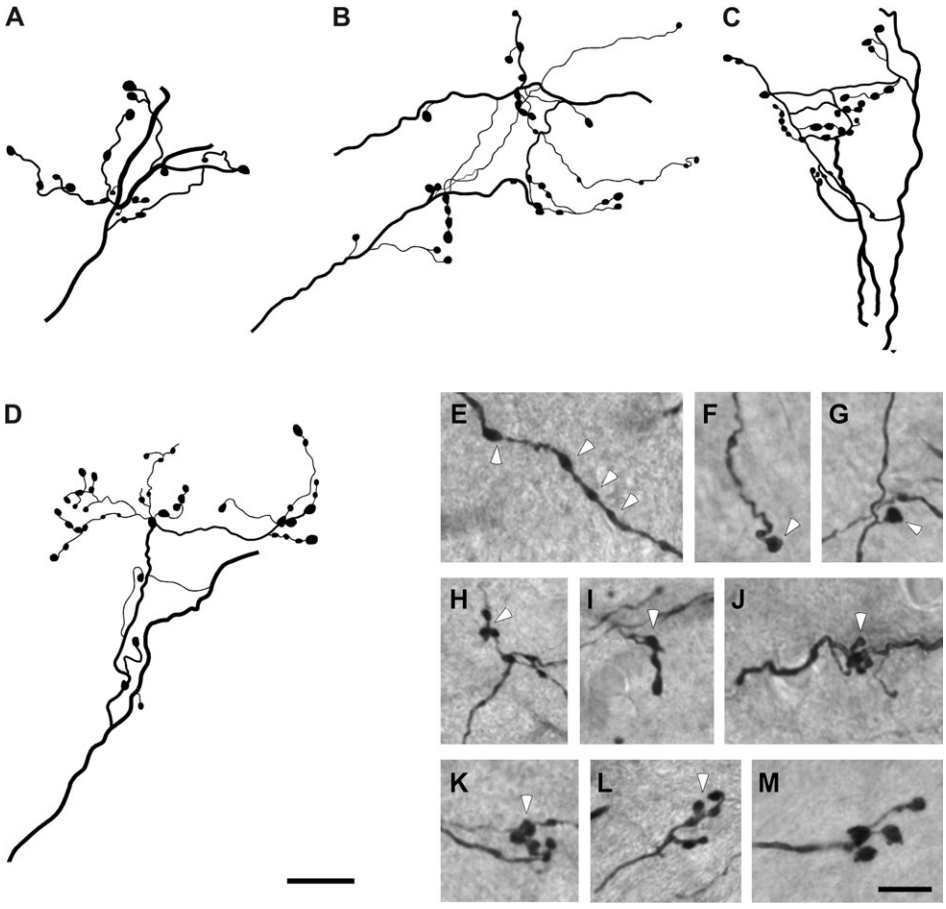

Figure 3. Examples of type 2 axon terminal fields in the deep layers of the SC. These axons were thicker than type 1 axons and presented more complex branching patterns and bouton groupings. They commonly ramified into branches that formed terminal arbors of varied complexity, where medium to large sized boutons were observed (*A–D*). These swellings were *en passant* boutons (arrowheads in *E*), boutons *terminaux* (arrowheads in *F*, *G*), as well as clustered boutons that may form rosette-like configurations or more complex structures (arrowheads in *H–M*). Scale bar = 25 μm in (*D*); 10 μm in (*M*).

multiple synaptic contacts with postsynaptic dendrites that were not apposed by other synaptic elements (Fig. 6*B,D*). In other instances, these terminals could also be seen presynaptic to SMI-32 immunostained dendritic profiles that received synaptic contacts from unstained terminals of unidentified origin (asterisks in Fig. 6*A,C,E*). Figure 6*E* shows 2 labeled cortico-collicular terminals from SIV that are presynaptic to a large longitudinally sectioned SMI-32 immunostained dendrite.

Convergence Patterns of Cortical Terminals onto SMI-32 Immunostained SC Neurons

To investigate the manner in which different AES subdivisions converge onto individual SC output neurons, paired injections of 2 different fluorescent tracers were made into AES subdivisions that were delineated based on electrophysiological criteria (Figs 7–9; also see Methods for a detailed description of triple-labeling studies).

FAES–AEV

After paired FAES and AEV injections, labeled fibers (red from FAES; green from AEV) appositions were evident both across different compartments (Fig. 7*A*) and within a single compartment (yellow asterisk in Fig. 7*B*) of an SMI-32 immunostained neuron. Appositions were seen on the soma ("s" in Fig. 7) as well as on primary, secondary, and tertiary dendrites (1, 2, or 3, respectively, in Fig. 7). Output neurons receiving these convergent projections from the auditory and visual subregions of AES were generally of large and intermediate size and either multipolar or bipolar in shape (Fig. 7*A,B*). Their soma diameters ranged from 25 to 70 μm with a mean diameter of 44.18 ± 0.99 μm with peaks between 40 and 55 μm (Fig. 7*C*), consistent with the known morphology of SC output neurons (Fuentes-Santamaria et al. 2006).

The distance of each apposition from the SMI-32 immunostained neuron's center was measured and revealed that those associated with FAES or AEV were located at similar distances regardless of whether they were observed on the soma, or primary, secondary or tertiary dendrite (ANOVA, $F_{3,437} = 2.32$, $P > 0.05$; Fig. 7*D*). The highest percentage of appositions was seen on primary dendrites (55–57%). Progressively lower percentages were observed on the soma (23–25%), secondary (15–17%), and tertiary (3%) dendrites (Fig. 7*E*). Statistical analyses showed that no significant differences were observed in the percentage of these appositions for each neuronal compartment (ANOVA, $F_{3,590} = 0.195$, $P > 0.05$).

AEV–SIV

The AEV–SIV (green from AEV; red from SIV) convergence patterns were strikingly similar to those described above (Figs 7 and 8). Appositions also were seen across different

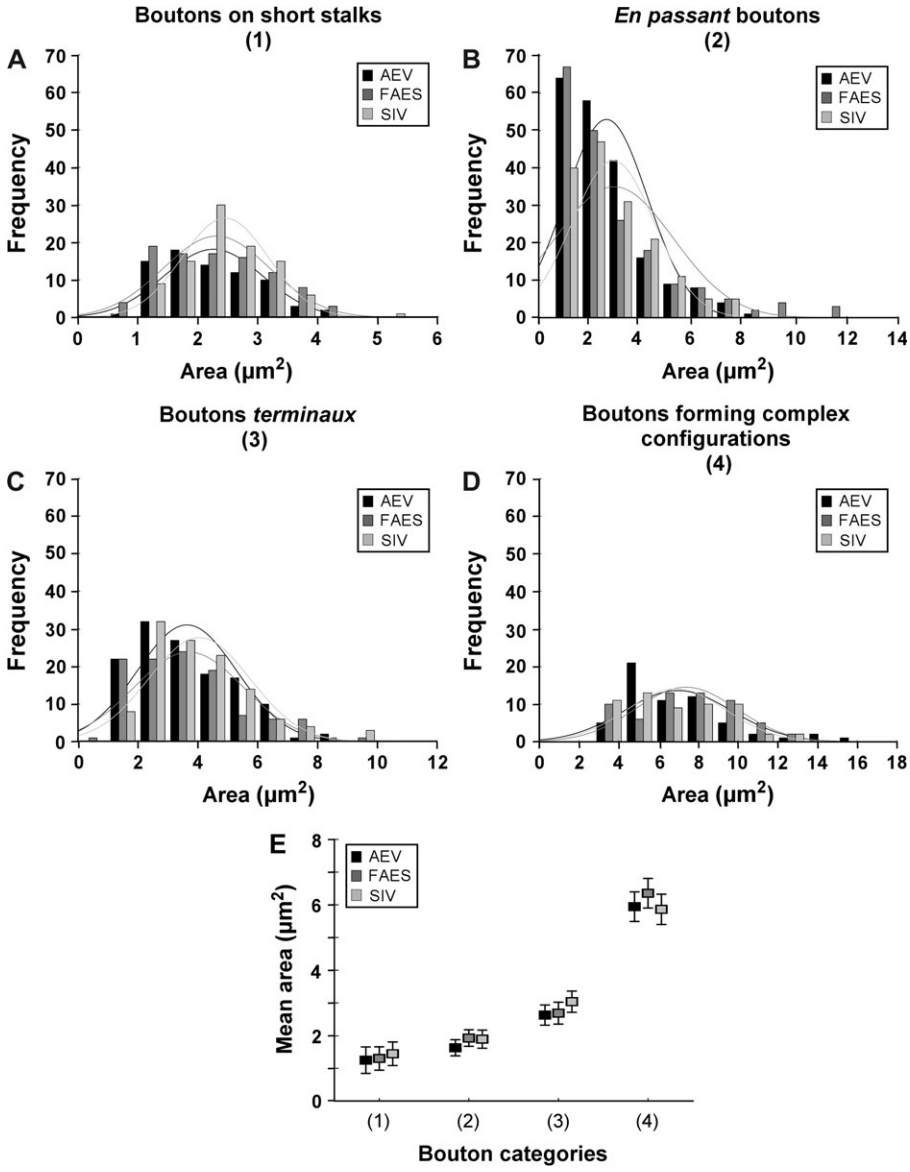

Figure 4. Histograms show the area of boutons from FAES, AEV and SIV for each category. Note that no significant differences in the area size of boutons on short stalks (*A*), *en passant* boutons (*B*), boutons *terminaux* (*C*), as well as boutons forming complex configurations (*D*) were observed among AES subdivisions. Comparisons among the mean areas for each bouton category are shown in (*E*). Notice that boutons on short stalks had the smallest areas while clustered boutons had the largest.

compartments (Fig. 8*A*) and within a single compartment (yellow asterisk in Fig. 8*B*), and were distributed on the soma and dendrites of SC SMI-32 immunostained neurons. These neurons had similar morphologies and soma sizes as those targeted by FAES and AEV (Fig. 8*C*). In addition, appositions from AEV and SIV were located at similar distances from the target neuron's center (ANOVA, $F_{3,437} = 2.32$, $P > 0.05$; Fig. 8*D*) and were found with equal frequency on SC target neurons with the highest percentage on primary dendrites and progressively lower percentages on the soma, secondary and tertiary dendrites (ANOVA, $F_{3,590} = 0.195$, $P > 0.05$; Fig. 8*E*).

FAES–SIV

Appositions from FAES (green) and SIV (red) also were found across (Fig. 9*A*) and within (yellow asterisk in Fig. 9*B*) neuronal compartments of targeted SC output neurons whose morphology and size did not differ significantly (Fig. 9*C*) from those described above for the FAES–AEV (Fig. 7*C*) and AEV–SIV (Fig. 8*C*) convergence patterns (ANOVA, $F_{2,151} = 2.78$, $P > 0.05$). Likewise, appositions from FAES and SIV were distributed similarly in terms of their respective distance from the soma center (ANOVA, $F_{3,124} = 0.05$, $P > 0.05$; Fig. 9*D*), and frequency on a given neuronal compartment (ANOVA, $F_{3,200} = 0.026$, $P > 0.05$; Fig. 9*E*).

No group differences among the 3 convergence patterns were noted either in the distribution of appositions in terms of their distance from the soma center (ANOVA, $F_{3,854} = 0.77$, $P > 0.05$) or in the percentage of these appositions within each neuronal compartment (ANOVA, $F_{3,1222} = 0.07$, $P > 0.05$), indicating that there were remarkable similarities in the projections arising from these different AES subregions and in their convergence patterns on their target neurons in the SC.

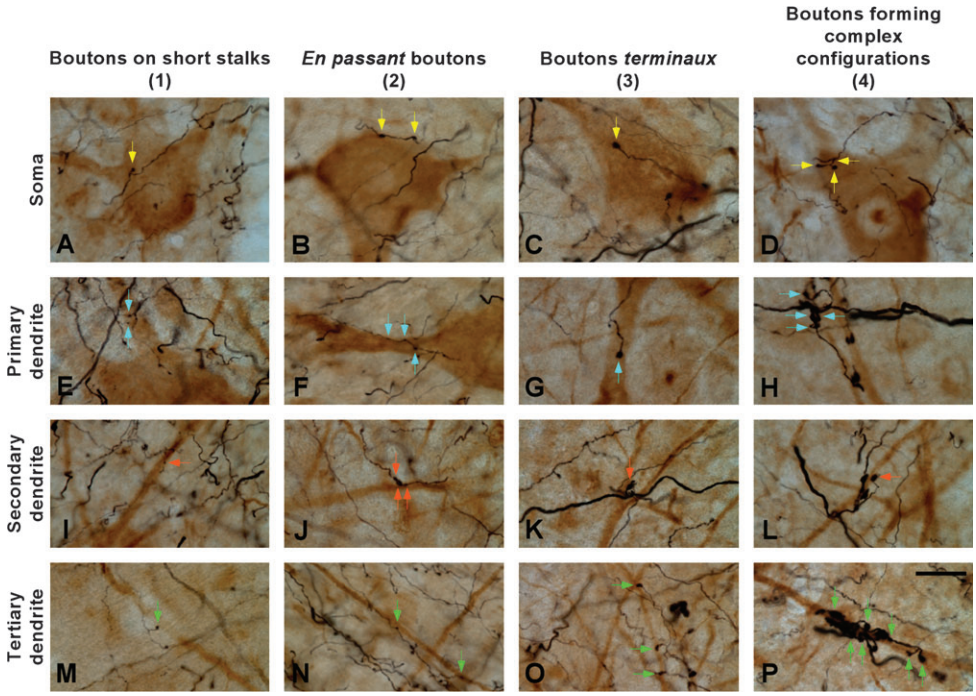

Figure 5. Boutons from AES subdivisions appose SMI-32 immunostained neurons. The soma (*A–D*) as well as the primary (*E–H*), secondary (*I–L*), and tertiary (*M–P*) dendrites of SMI-32 immunostained neurons were apposed by boutons with different morphology and size, including those linked to thin axons by short stalks (*A*, *E*, *I*, and *M*), *en passant* boutons (*B*, *F*, *J*, and *N*), boutons *terminaux* (*C*, *G*, *K*, and *O*) and boutons with more complex configuration (*D*, *H*, *L*, and *P*). Arrows indicate cortical appositions on each neuron compartment. Scale bar = 25 μm in (*P*).

Discussion

The present data provide the first anatomical demonstration that afferents from modality-specific subdivisions along the AES converge onto individual deep layer SC output neurons. These observations further reveal that such convergence is conveyed by 2 distinct morphological types of axon terminals that are reminiscent of those previously described in corticothalamic projections from sensory and motor cortex (Sherman and Guillery 1998; Guillery et al. 2001; Kultas-Ilinsky et al. 2003; Huppé-Gourgues et al. 2006). Nevertheless, despite the apparent conservation of axonal morphologies across different cortical-subcortical systems, there is not a clear cut adaptation of the concomitant physiological attributes ascribed to type I and II fibers in the visual thalamus to the cortico-collicular projection. These issues, and the potential implications for understanding the physiology of cortically mediated multisensory integration in the SC, are discussed in greater detail below.

Type I and Type II Cortical-Collicular Axons

Two morphological categories of AES cortico-collicular axons were apparent. Type I were small-caliber axons that traversed long distances within the SC without branching. Such axons bore mainly small boutons on thin short stalks, widely-spaced *en passant* swellings and/or single boutons *terminaux;* these characteristics defined the majority of AES cortico-collicular fibers in the deep SC. By contrast, a considerably smaller proportion of AES afferents had thicker axons that often displayed more complex branching patterns in the region of their terminal arbors. These type II axons also typically had larger boutons than were the boutons associated with type I axons. Both type I and type II axons originated from neurons in AEV, FAES, and SIV, and no apparent area-specific differences in their relative incidences or morphological features were observed.

As noted earlier, type I and type II morphologies are not unique features of AES cortico-collicular projections but have been described previously in the corticothalamic pathways arising from both sensory (Sherman and Guillery, 1998; Guillery et al. 2001; Huppé-Gourgues et al. 2006) and motor (Kultas-Ilinsky et al. 2003) regions. In contemporary schemes of corticothalamic influences these 2 morphological types subserve distinct functional roles (for review, see Guillery and Sherman 2002; Sherman and Guillery 2002; Sherman 2007) wherein type I axons are believed to provide "modulatory" inputs and type II contribute "driver" inputs to visual thalamocortical neurons. The former effects modulation via small graded postsynaptic potentials and the latter drives thalamic neurons with faster, larger postsynaptic potentials (Sherman and Guillery 1996; Guillery et al. 2001; Reichova and Sherman 2004).

Despite the morphological similarities between cortico-thalamic and cortico-collicular axons, it is not clear to what extent the functional schema envisioned for sensory interactions in the thalamus is applicable to multisensory processing in the SC. Because AES exerts a critical influence over multisensory integration in SC neurons (Wallace and Stein 1994; Jiang et al. 2001; Alvarado et al. 2007), it is tempting to assume that these morphologic-specific functional properties extend to the cortico-collicular system. Thus, although deactivation of AES abolishes the characteristic integrated responses of SC neurons to cross-modal stimuli, it generally does not eliminate their responsiveness to the modality-specific

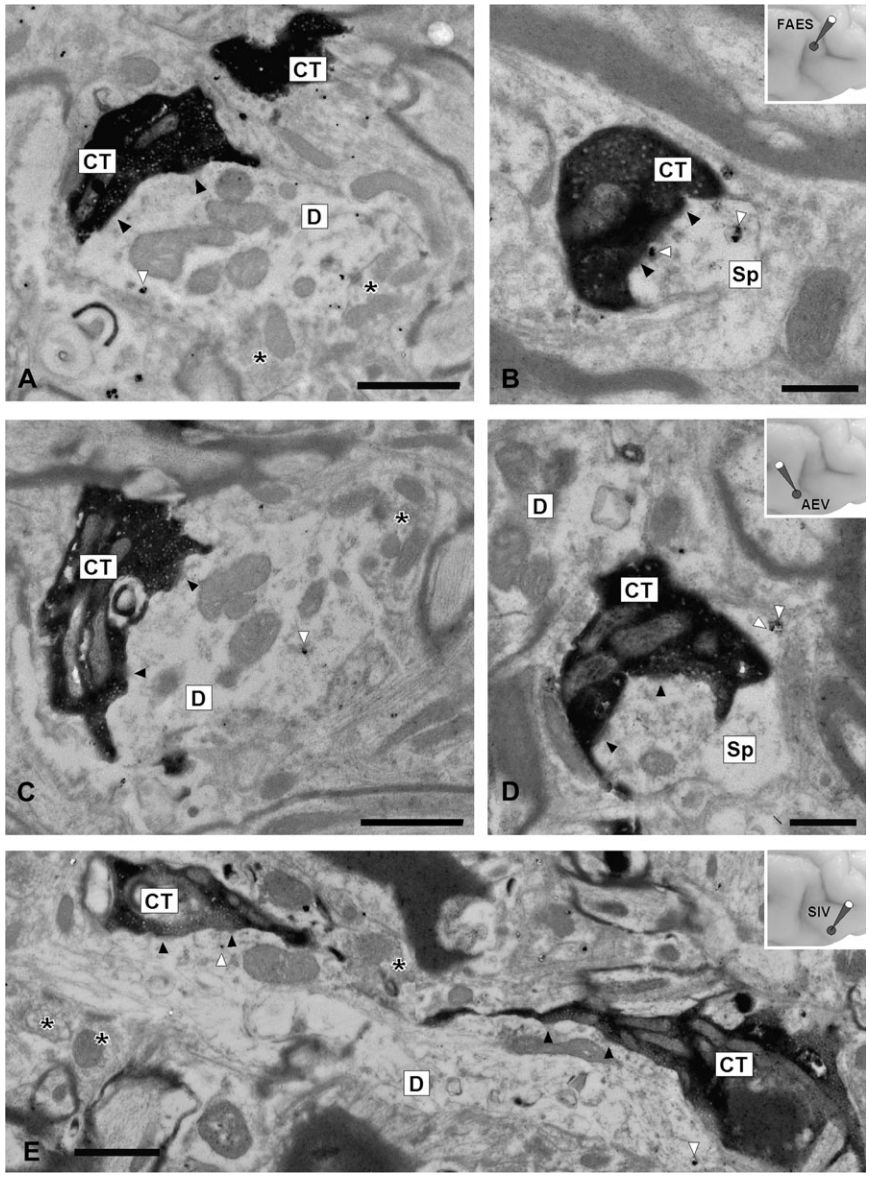

Figure 6. Ultrastructure of AES terminals and their relationships to SMI-32 immunostained neurons. Injections of BDA were made into FAES (*A*, *B*), AEV (*C*, *D*), and SIV (*E*) to anterogradely label terminals into the deep layers of the SC. These boutons made asymmetrical synaptic contacts with modest postsynaptic densities (black arrowheads) and were presynaptic to SMI-32 immunostained dendrites labeled with silver-intensified immunogold labeled particles (white arrowheads). Notice that stained dendrites were also apposed by numerous unstained elements (asterisks). Abbreviations: CT, cortical terminal; D, stained dendrite; Sp, dendritic spine. Scale bars = 1 μm in *A* (also applies to *C*); 0.5 μm in (*B*) and (*D*); 1 μm in (*E*).

component stimuli (Wallace and Stein 1994; Jiang et al. 2001; Alvarado et al. 2007). Similarly, AES deactivation abolishes multisensory enhancements in behavioral performance without compromising performance in responses to modality-specific targets (Wilkinson et al. 1996; Jiang et al. 2002). Nevertheless, in some, albeit a minority, of instances AES does appear to function as a driver by being primarily responsible for the sensory responses of some SC neurons (Wallace and Stein 1994; Jiang et al. 2001; Alvarado et al. 2007). This lower incidence of driver-like influences from AES would, therefore, be consistent with the low incidence of type II axons in the AES cortico-collicular projection.

However, the utility of generalizing the corticothalamic schema to the present context is mitigated by several anatomical distinctions between these 2 corticofugal systems. First, there are differences with regard to their lamina of origin and the soma sizes of the originating cortical neurons. In cortico-collicular pathways, including those originating in cat AES, the neurons of origin are restricted to layer V (Kawamura and Konno 1979, Tortelly et al. 1980; Stein et al. 1983; McHaffie et al. 1988; Meredith and Clemo 1989). By contrast, type I and type II corticothalamic axons in rat have different laminar sources such that type I axons arise from small soma neurons in layer VI and type II originate from large soma layer V neurons (Bourassa and Deschenes 1995). Although both medium and large soma neurons give rise to cortico-collicular afferents in cats, the medium neurons are far more numerous than their large layer V counterparts regardless of the cortical region of origin (Kawamura and Konno 1979). Given the relative occurrence of type I and type II axons originating in AES, it is

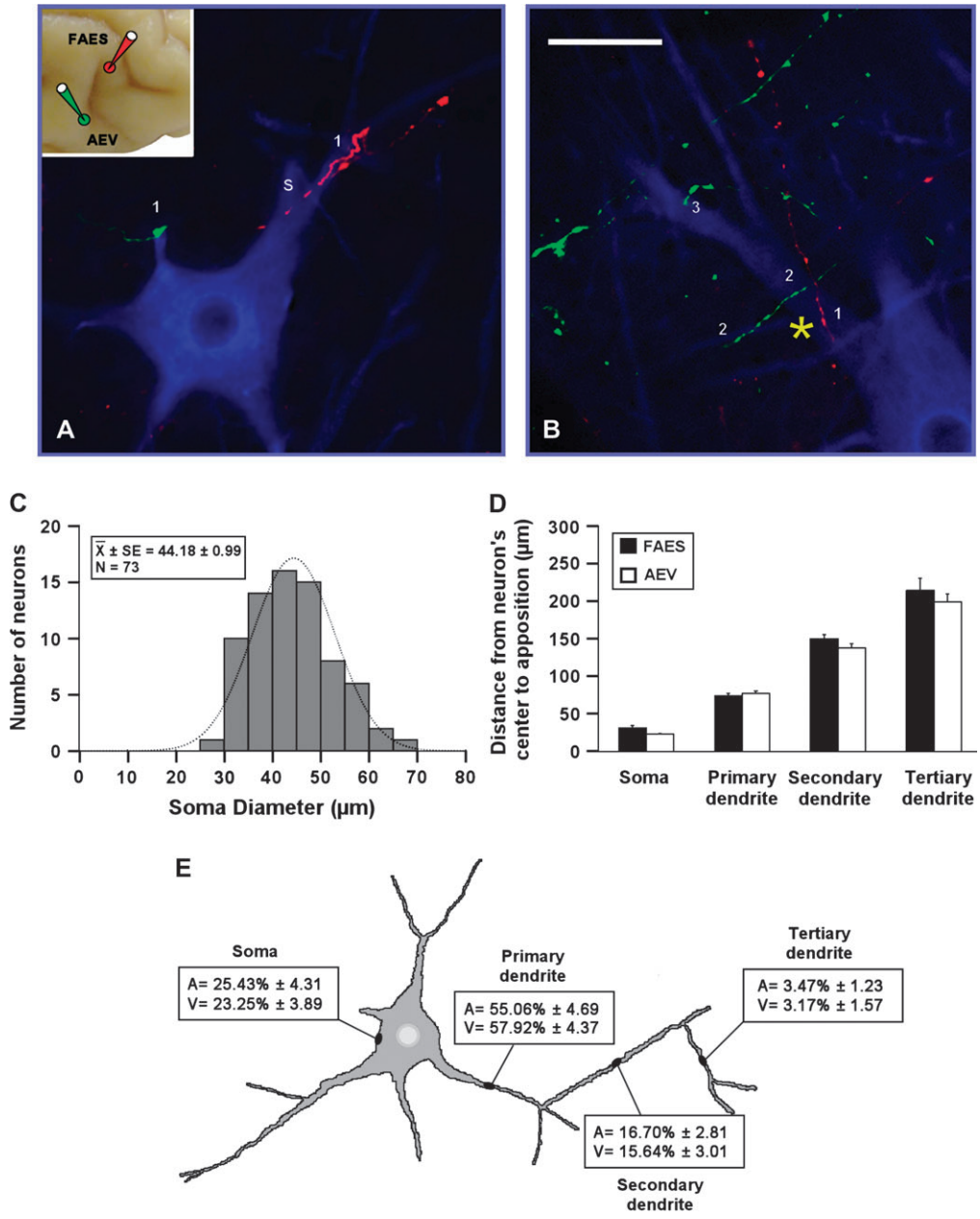

Figure 7. Modality-convergence pattern of FAES–AEV onto SMI-32 immunostained neurons. Injections of BDA were made into FAES and AEV (see inset at the left top corner in *A*) in order to anterogradely label fibers from FAES (red) and AEV (green). Appositions from each modality-specific subdivision were observed either across the different compartments (*A*) or within a single compartment (yellow asterisk in *B*) of the SMI-32 immunostained neuron. They distributed on the soma ("s") as well as on primary ("1"), secondary ("2"), and tertiary ("3") dendrites of SMI-32 immunostained neurons (*A*, *B*). The distribution of the soma diameters of neurons receiving convergent inputs from FAES and AEV is shown in (*C*). Notice that these neurons are mainly large in size with a mean diameter of 44.18 ± 0.99. Appositions from FAES and AEV were located at similar distances on the cell body as well as on dendrites (*D*). The highest percentage of these appositions was observed on primary dendrites and less commonly on the cell body, secondary and tertiary dendrites (*E*). No significant differences were observed either in the distribution or in the percentage of appositions from FAES–AEV onto the SMI-32 immunostained neuron's compartments. Scale bar = 50 μm in B.

not unreasonable to speculate that the 2 types arise from medium and large neurons, respectively. Whether these 2 AES populations convey different information is not known. However, in lateral suprasylvian visual cortex, cortico-collicular afferents preferentially arise from large layer V neurons that are segregated from those small to medium layer V neurons that give rise to corticostriatal afferents (Norita et al. 1991; McHaffie et al. 1993). In this instance, each segregated corticofugal population has distinct physiological properties (Niida et al. 1997).

A second distinction between these 2 corticofugal systems is that corticothalamic types I and II afferents have differential spatial distributions along the dendritic arbors of thalamic neurons, with the former having small terminals that form single contacts with distal dendrites and the latter having large terminals that establish multiple contacts onto proximal dendrites (for review see Sherman and Guillery 1996; Sherman 2007). Presumably, these anatomical distinctions mediate their differing functional roles. No such differential distribution was noted however, in type I and type II cortico-collicular axons

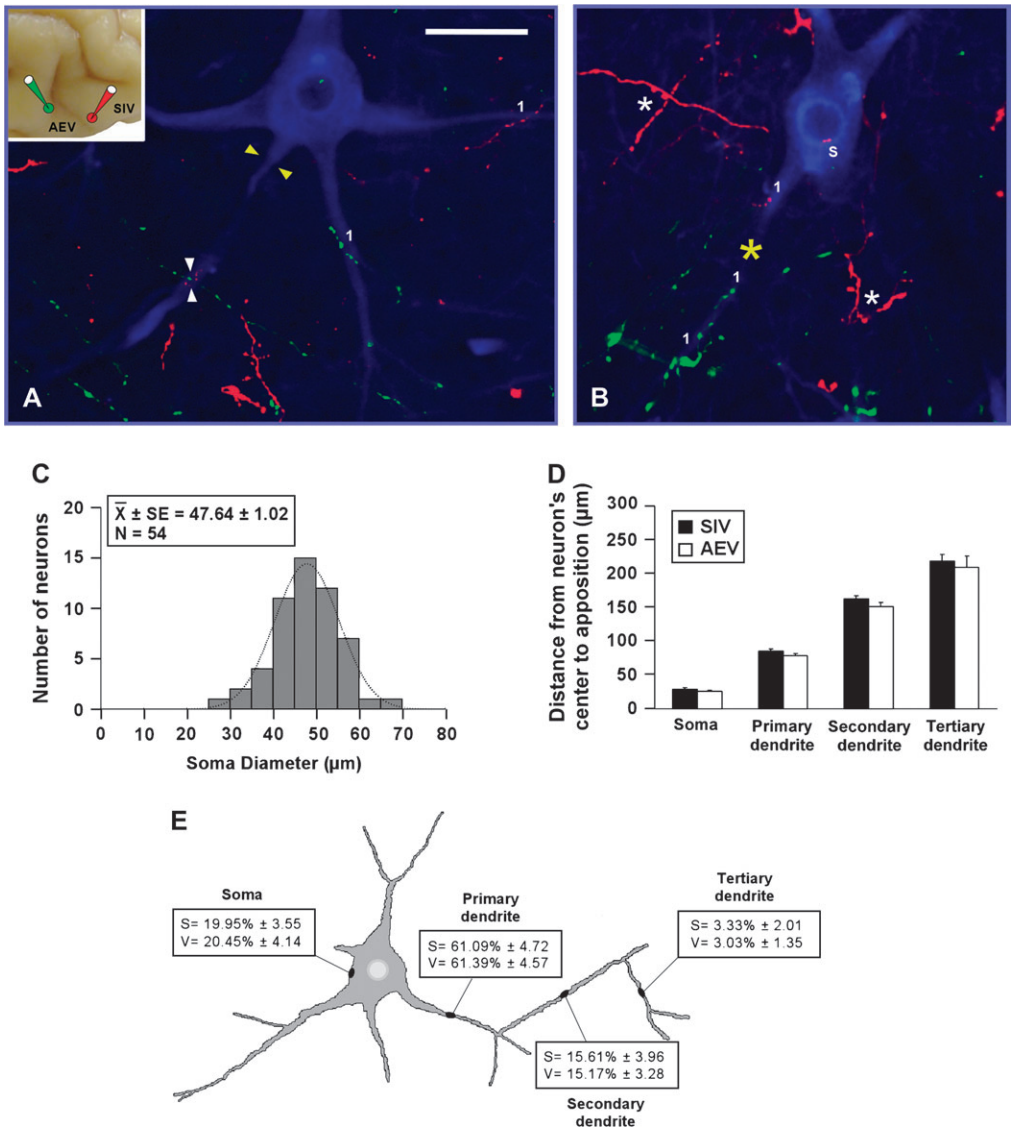

Figure 8. Modality-convergence pattern of AEV–SIV onto SMI-32 immunostained neurons. Anterogradely labeled fibers from AEV (green) and SIV (red) were observed either across the different compartments (*A*) or within a single compartment (yellow asterisk in *B*) of the SMI-32 immunostained neuron. Appositions distributed on the soma ("s") as well as on primary ("1"), secondary ("2"), and tertiary ("3") dendrites of SMI-32 immunostained neurons (*A*, *B*). The soma diameters of neurons receiving convergent inputs from AEV and SIV are shown in (*C*). Appositions from AEV and SIV were located at similar distances on the cell body as well as on dendrites (*D*), and the highest percentage of appositions was observed on primary dendrites and less frequently on the other neuron's compartments (*E*). No significant differences were observed either in the distribution or in the percentage of appositions from AEV–SIV onto the SMI-32 immunostained neuron's compartments. Scale bar = 50 μm in (*A*).

from AES. Further studies will be necessary to determine whether type I and type II cortico-collicular axons arise from heterogeneous populations of layer V neurons in AES, and whether different afferent sources are associated with different physiological properties.

On the other hand, it might be argued that the relevant AES axon terminals most closely associated with SC multisensory integration are the less frequently occurring type IIs. A recent model of SC multisensory integration (Rowland et al. 2007) relies, in part, on the clustering of cortico-collicular afferents from different AES subdivisions within the same electrotonic compartments where they are associated with α-Amino-3-hydroxy-5-methyl-4-isoxazole-propionic acid and N-methyl-D-aspartate receptors. The large boutons and clustered terminals configurations that characterize type II AES terminals seem ideally suited to make maximum use of these receptors and thus, exert the greatest impact on the physiology of their target SC neurons. Moreover, given the rather delayed postnatal onset of SC multisensory integration capabilities development (Wallace and Stein 1997), one might postulate that type II axons would appear much later than their type I counterparts. Indeed, preliminary observations suggest that neonatal AES projections are characterized by thin linear axons with few large boutons (Jiang et al. 2003). Although the point in postnatal maturation at which larger, more complex type II–like AES fibers first appear has not yet been established, those AES fibers in the juvenile cat SC contain complex terminal arbors with large boutons by 3 postnatal months, a time at which SC multisensory integration more closely approximates the adult condition and is dependent on AES influences (Wallace and Stein 1997; Wallace and Stein 2000). It is also interesting to note that type II axons in cat corticothalamic projections (from lateral suprasylvian to the

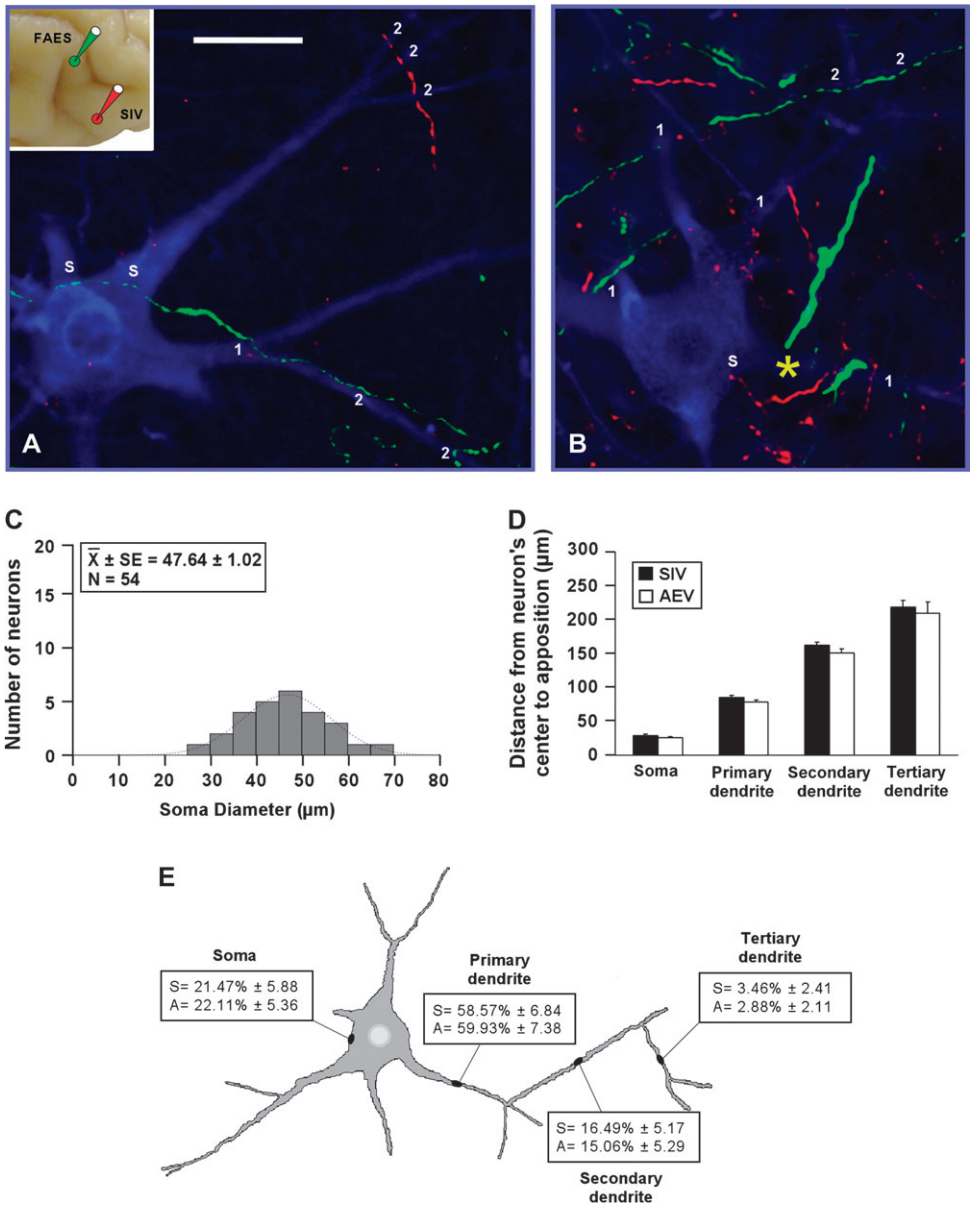

Figure 9. Modality-convergence pattern of FAES–SIV onto SMI-32 immunostained neurons. Appositions from each modality-specific subdivision (red for FAES; green for SIV) also were observed either across the different compartments (*A*) or within a single compartment (yellow asterisk in *B*) of the SMI-32 immunostained neuron. They distributed on the soma ("s") as well as on primary ("1"), secondary ("2"), and tertiary ("3") dendrites of SMI-32 immunostained neurons (*A*, *B*). The distribution of the soma diameters of neurons receiving convergent inputs from FAES and SIV is shown in (*C*). Appositions from FAES and SIV were located at similar distances on the cell body as well as on dendrites (*D*), with the highest percentage of appositions being on primary dendrites (*E*). No significant differences were observed either in the distribution or in the percentage of appositions from FAES–SIV onto SMI-32 immunostained neuron compartments. Scale bar = 50 µm in (*A*).

lateral posterior complex, Matsumoto et al. 2006) first appear at 30 days postnatal, the same time that multisensory integration first appears in SC neurons (Wallace and Stein 1997).

Terminal Patterns of AES Projections onto SC Neurons

Previously, Harting et al. (1997) compared how descending cortico-collicular afferents from SIV and ascending modality-specific inputs from the trigeminal nucleus terminated on SC neurons. Using the diameter of postsynaptic dendrites as an index of synapse location, these investigators concluded that cortico-collicular synapses terminate on larger, presumably proximal dendrites of output neurons, whereas trigemino-collicular synapses terminate on smaller, presumably distal dendrites. They suggested that the morphology, size, and location of the cortical synapses might be critical in their role of mediating SC multisensory integration. However, the present observations failed to detect any differential spatial distribution of labeled boutons onto the dendrites of SC output neurons. Because the dendritic arbor was continuously labeled, there was no doubt about the particular dendrite contacted by an AES input. Indeed, primary, secondary and even tertiary dendrites were contacted by complex bouton configurations from all AES subdivisions, including SIV. The differences between the present findings and those of Harting et al. (1997) are likely due to the different methodologies employed. Earlier anatomical techniques may have biased the sample toward larger synapses and were unable to provide an unequivocal means for determining the nature of the postsynaptic element.

Though well suited to dealing with the issue discussed above, the present techniques are limited in their utility for evaluating the fine details with which projections from different AES subdivisions converge on common target neurons. Bulk filling pairs of subdivisions does not guarantee matching topographical features that determine terminal projection patterns onto these common pools of SC neurons. Nevertheless, in some instances, afferents from 2 AES subdivisions were seen terminating in close proximity to one another on the soma or within a common area of a given SC neuron's dendritic arbor. This convergence pattern is consistent with predictions of a recent neural network model based on other physiological and anatomical findings (Rowland et al. 2007). Fundamental to the model is the assumption that the functional impact of AES on SC multisensory integration depends on the convergence of inputs from 2 or more of its unisensory subdivisions onto the same electrotonic compartment of an SC neuron. The model links the observed anatomical features to an explanation of the apparent synergy among these projections, wherein deactivation of either one is sufficient to compromise multisensory integration (Wallace and Stein 1994; Alvarado et al. 2006). Another prediction of the model, a divisive inhibition produced by local interneurons, has recently been supported by findings that AES projections also target nitric oxide containing SC interneurons, many of which also contain the inhibitory neurotransmitter γ-aminobutyric acid and project onto output neurons (Fuentes-Santamaria et al. 2008).

Summary

The phenomenological principles that characterize multisensory integration in the SC (Stein and Meredith 1993) ultimately rely not simply on the intrinsic physiological characteristics of individual multisensory SC neurons themselves but also on the cortical information which is conveyed, either directly or indirectly through intrinsic SC interneurons, onto these SC output neurons (Fuentes-Santamaria et al. 2008). Moreover, the different morphological axon types detailed here, and their corresponding presumptive physiological differences in synaptic physiology, indicate that this transformation has levels of complexity not previously recognized. Although our understanding of the physiological, pharmacological and neurochemical basis of integration is far from complete, the complexity of cortico-collicular architecture subserving multisensory integration is one that suggests nonlinear synaptic transformations that contribute to nonlinear SC responses. How these various anatomical features contribute to the "rules" governing multisensory integration (inverse effectiveness, response suppression, spatial rule) will be important aspects to address in the future.

Funding

National Institutes of Health (grant numbers NS36916 and EY016716) to B.E.S and (NS35008) to J.G.M.; The Wallace Research Foundation grant.

Notes

We thank Drs M. Willingham, K. Grant, P. Moore, and B. Dawson for their expert electron microscopy assistance and N. London for editorial assistance. *Conflict of Interest*: None declared.

Address correspondence to Dr Veronica Fuentes-Santamaria, Regional Center for Biomedical Research, Department of Medical Sciences, School of Medicine, University of Castilla-La Mancha, Albacete, Spain. Email: Veronica.Fuentes@uclm.es.

References

Alvarado JC, Stanford TR, Vaughan JW, Stein BE. 2006. Synergy among the cortico-collicular influences underlying multisensory integration. Program No. 639.5. Neuroscience Meeting Planner. Atlanta (GA): Society for Neuroscience.

Alvarado JC, Stanford TR, Vaughan JW, Stein BE. 2007. Cortex mediates multisensory but not unisensory integration in superior colliculus. J Neurosci. 27(47):12775–12786.

Bourassa J, Deschenes M. 1995. Corticothalamic projections from the primary visual cortex in rats: a single fiber study using biocytin as an anterograde tracer. Neuroscience. 66(2):253–263.

Burnett LR, Stein BE, Chaponis D, Wallace MT. 2004. Superior colliculus lesions preferentially disrupt multisensory orientation. Neuroscience. 124(3):535–547.

Burry RW. 2000. Specificity controls for immunocytochemical methods. J Histochem Cytochem. 48(2):163–166.

Clarey JC, Irvine DR. 1986. Auditory response properties of neurons in the anterior ectosylvian sulcus of the cat. Brain Res. 386(1–2):12–19.

Clemo HR, Stein BE. 1982. Somatosensory cortex: a 'new' somatotopic representation. Brain Res. 235:162–168.

Clemo HR, Stein BE. 1983. Organization of a fourth somatosensory area of cortex in cat. J Neurophysiol. 50(4):910–925.

Edwards SB, Ginsburgh CL, Henkel CK, Stein BE. 1979. Sources of subcortical projections to the superior colliculus in the cat. J Comp Neurol. 184:309–330.

El Manira A, Zhang W, Svensson E, Bussieres N. 1997. 5-HT inhibits calcium current and synaptic transmission from sensory neurons in lamprey. J Neurosci. 17(5):1786–1794.

Fuentes-Santamaria V, Stein BE, McHaffie JG. 2006. Neurofilament proteins are preferentially expressed in descending output neurons of the cat the superior colliculus: a study using SMI-32. Neuroscience. 138(1):55–68.

Fuentes-Santamaria V, Alvarado JC, Stein BE, McHaffie JG. 2008. Cortex contacts both output neurons and nitrergic interneurons in the superior colliculus: direct and indirect routes for multisensory integration. Cereb Cortex. 18:1640–1652.

Grantyn A, Grantyn R. 1982. Axonal patterns and sites of termination of cat superior colliculus neurons projecting in the tecto-bulbo-spinal tract. Exp Brain Res. 46:243–256.

Guillery RW. 1966. A study of Golgi preparations from the dorsal lateral geniculate nucleus of the adult cat. J Comp Neurol. 128:21–50.

Guillery RW, Feig SL, Van Lieshout DP. 2001. Connections of higher order visual relays in the thalamus: a study of corticothalamic pathways in cats. J Comp Neurol. 438:66–85.

Guillery RW, Sherman SM. 2002. Thalamic relay functions and their role in corticocortical communication: generalizations from the visual system. Neuron. 33(2):163–175.

Guitton D, Munoz DP. 1991. Control of orienting gaze shifts by the tectoreticulospinal system in the head-free cat. I. Identification, localization, and effects of behavior on sensory responses. J Neurophysiol. 66:1605–1623.

Harting JK, Feig S, Van Lieshout DP. 1997. Cortical somatosensory and trigeminal inputs to the cat superior colliculus: light and electron microscopic analyses. J Comp Neurol. 388(2):313–326.

Huerta MF, Harting JK. 1982. Tectal control of spinal cord activity: neuroanatomical demonstration of pathways connecting the superior colliculus with the cervical spinal cord grey. Prog Brain Res. 57:293–328.

Huerta MF, Harting JK. 1984. The mammalian superior colliculus: studies of its morphology and connections. In: Vanegas H, editor. Comparative neurology of the optic tectum. New York: Plenum Press. p. 687–773.

Huppé-Gourgues F, Bickford ME, Boire D, Ptito M, Casanova C. 2006. Distribution, morphology, and synaptic targets of corticothalamic terminals in the cat lateral posterior-pulvinar complex that originate from the posteromedial lateral suprasylvian cortex. J Comp Neurol. 497(6):847–863.

Jiang W, Wallace MT, Jiang H, Vaughan JW, Stein BE. 2001. Cortical areas mediate multisensory integration in superior colliculus neurons. J Neurophysiol. 85(2):506–522.
Jiang W, Jiang H, Stein BE. 2002. Two corticotectal areas facilitate multisensory orientation behavior. J Cogn Neurosci. 14(8):1240–1255.
Jiang W, Jiang H, McHaffie JG, Stein BE. 2003. Protracted maturation of Corticotectal projections is responsible for the development of Multisensory integration in the superior colliculus. Program No. 267.14. Abstract Viewer/Itinerary Planner. Washington (DC): Society for Neuroscience.
Kanaseki T, Sprague JM. 1974. Anatomical organization of pretectal nuclei and tectal laminae in the cat. J Comp Neurol. 158:319–337.
Kawamura K, Konno T. 1979. Various types of corticotectal neurons of cats as demonstrated by means of retrograde axonal transport of horseradish peroxidase. Exp Brain Res. 35(1):161–175.
Kultas-Ilinsky K, Sivan-Loukianova E, Ilinsky IA. 2003. Reevaluation of the primary motor cortex connections with the thalamus in primates. J Comp Neurol. 457(2):133–158.
Lee VM, Otvos L, Carden MJ, Hollosi M, Dietzschold B, Lazzarini RA. 1988. Identification of the major multiphosphorylation site in mammalian neurofilaments. Proc Natl Acad Sci USA. 6:1998–2002.
Makeham JM, Goodchild AK, Pilowsky PM. 2001. NK1 receptor and the ventral medulla of the rat: bulbospinal and catecholaminergic neurons. Neuroreport. 12(17):3663–3667.
Matsumoto S, Hoshino K, Kobayashi K, Norita M. 2006. Postnatal development of the corticothalamic projections from the visual association cortex to the lateralis posterior complex in the cat. Acta Physiol Hungarica. 93(1):79–90.
McHaffie JG, Kruger L, Clemo HR, Stein BE. 1988. Corticothalamic and corticotectal somatosensory projections from the anterior ectosylvian sulcus (SIV cortex) in neonatal cats: an anatomical demonstration with HRP and 3H-leucine. J Comp Neurol. 274(1):115–126.
McHaffie JG, Norita M, Dunning DD, Stein BE. 1993. Corticotectal relationships: direct and "indirect" corticotectal pathways. Prog Brain Res. 95:139–150.
Meredith MA, Clemo HR. 1989. Auditory cortical projection from the anterior ectosylvian sulcus (field AES) to the superior colliculus in the cat: an anatomical and electrophysiological study. J Comp Neurol. 289(4):687–707.
Meredith MA, Wallace MT, Stein BE. 1992. Visual, auditory and somatosensory convergence in output neurons of the cat superior colliculus: multisensory properties of the tecto-reticulo-spinal projection. Exp Brain Res. 88(1):181–186.
Mucke L, Norita M, Benedek G, Creutzfeldt O. 1982. Physiologic and anatomic investigation of a visual cortical area situated in the ventral bank of the anterior ectosylvian sulcus of the cat. Exp Brain Res. 46(1):1–11.
Munoz DP, Guitton D. 1991. Control of orienting gaze shifts by the tectoreticulospinal system in the head-free cat. II. Sustained discharges during motor preparation and fixation. J Neurophysiol. 66:1624–1641.
Niida T, Stein BE, McHaffie JG. 1997. Response properties of corticotectal and corticostriatal neurons in the posterior lateral suprasylvian cortex of the cat. J Neurosci. 17(21):8550–8565.
Norita M, Mucke L, Albowitz B, Katoh Y, Creutzfeldt OD. 1986. Connections of the anterior ectosylvian visual area (AEV). Exp Brain Res. 62(2):225–240.
Norita M, McHaffie JG, Shimizu H, Stein BE. 1991. The corticostriatal and corticotectal projections of the feline lateral suprasylvian cortex demonstrated with anterograde biocytin and retrograde fluorescent techniques. Neurosci Res. 10(2):149–155.
Olson CR, Graybiel AM. 1987. Ectosylvian visual area of the cat: location, retinotopic organization, and connections. J Comp Neurol. 261(2): 277–294.
Pilowsky P, Llewellyn-Smith IJ, Lipski J, Chalmers J. 1992. Substance P immunoreactive boutons form synapses with feline sympathetic preganglionic neurons. J Comp Neurol. 320(1):121–135.
Reichova I, Sherman SM. 2004. Somatosensory corticothalamic projections: distinguishing drivers from modulators. J Neurophysiol. 4:2185–2197.
Rockland KS. 1996. Two types of corticopulvinar terminations: round (type 2) and elongate (type 1). J Comp Neurol. 368(1):57–87.
Rowland BA, Stanford TR, Stein BE. 2007. A model of the neural mechanisms underlying multisensory integration in the superior colliculus. Perception. 36(10):1431–1443.
Sherman SM, Guillery RW. 1996. Functional organization of thalamocortical relays. J Neurophysiol. 76(3):1367–1395.
Sherman SM, Guillery RW. 1998. On the actions that one nerve cell can have on another: distinguishing "drivers" from "modulators". Proc Natl Acad Sci USA. 95(12):7121–7126.
Sherman SM, Guillery RW. 2002. The role of the thalamus in the flow of information to the cortex. Philos Trans R Soc Lond B Biol Sci. 357(1428):1695–1708.
Sherman SM. 2007. The thalamus is more than just a relay. Curr Opin Neurobiol. 17(4):417–422.
Stein BE, Spencer RF, Edwards SB. 1982. Efferent projections of the neonatal superior colliculus: extraoculomotor-related brain stem structures. Brain Res. 239(1):17–28.
Stein BE, Spencer RF, Edwards SB. 1983. Corticotectal and corticothalamic efferent projections of SIV somatosensory cortex in cat. J Neurophysiol. 50(4):896–909.
Stein BE, Huneycutt WS, Meredith MA. 1988. Neurons and behavior: the same rules of multisensory integration apply. Brain Res. 448(2): 355–358.
Stein BE, Meredith MA, Huneycutt WS, McDade L. 1989. Behavioral indices of multisensory integration: orientation to visual cues is affected by auditory stimuli. J Cogn Neurosci. 1:12–24.
Stein BE, Meredith MA. 1993. The merging of the senses. Cambridge (MA): MIT Press.
Stein BE, Meredith MA. 1991. Functional organization of the superior colliculus. In: Leventhal AG, editor. The neural bases of visual function. Hampshire (UK): Macmillan. p. 85–110.
Stein BE, Stanford TR. 2008. Multisensory integration: current issues from the perspective of the single neuron. Nat Rev Neurosci. 9(4):255–266.
Sternberger LA, Sternberger NH. 1983. Monoclonal antibodies distinguish phosphorylated and nonphosphorylated forms of neurofilaments in situ. Proc Natl Acad Sci USA. 19:6126–6130.
Tortelly A, Reinoso-Suarez F, Llamas A. 1980. Projections from non-visual cortical areas to the superior colliculus demonstrated by retrograde transport of HRP in the cat. Brain Res. 188(2):543–549.
Van der Gucht E, Vandesande F, Arckens L. 2001. Neurofilament protein: a selective marker for the architectonic parcellation of the visual cortex in adult cat brain. J Comp Neurol. 441(4):345–368.
Wallace MT, Meredith MA, Stein BE. 1993. Converging influences from visual, auditory, and somatosensory cortices onto output neurons of the superior colliculus. J Neurophysiol. 69(6):1797–1809.
Wallace MT, Stein BE. 1994. Cross-modal synthesis in the midbrain depends on input from cortex. J Neurophysiol. 71(1):429–432.
Wallace MT, Stein BE. 1997. Development of multisensory neurons and multisensory integration in cat superior colliculus. J Neurosci. 17:2429–2444.
Wilkinson LK, Meredith MA, Stein BE. 1996. The role of anterior ectosylvian cortex in cross-modality orientation and approach behavior. Exp Brain Res. 112(1):1–10.
Wallace MT, Stein BE. 2000. Onset of cross-modal synthesis in the neonatal superior colliculus is gated by the development of cortical influences. J Neurophysiol. 83:3578–3582.